Research Article

In Silico Validation of Emodin, Aloe-Emodin and Rhein Derivatives as Dermatological Cosmeceuticals for Anti-Aging, Anti-Acne, Anti-Pigmentation and Anti-Inflammatory Therapy

S K Vidhya Bharathi, A Kalpana*
PG & Research Department of Chemistry, Sri Sarada College for Women, Salem, Tamil Nadu 636 016, India.
***Corresponding author's E-mail:** kalpanaanbarasu@gmail.com

Received: 11-05-2026; **Revised:** 23-07-2026; **Accepted:** 28-07-2026; **Published online:** 20-08-2026.

ABSTRACT

Anthraquinone-based hybrids derived from emodin, aloe-emodin, and rhein were evaluated for their anti-aging, anti-acne, anti-pigmentation and anti-inflammatory activities. The compounds are systematically validated through in silico molecular docking and ADMET analysis to explore their potential as multifunctional cosmeceutical agents. Emodin derivatives are best suited for anti-aging and anti-acne applications due to their balanced ADMET profiles and effective skin penetration, while aloe-emodin hybrids favour anti-pigmentation and anti-inflammatory activities through enhanced dermal retention and safety. Rhein derivatives exhibit the highest multi-target potential with tunnable ADMET properties, making them ideal for broad-spectrum cosmeceutical applications. Docking studies revealed that rhein derivatives exhibit the strongest multi-target binding affinities across all the proteins, with compounds 33 and 55 emerging as the most potent leads. Aloe-emodin–coumarin hybrids showed consistently high interaction strength, while emodin derivatives demonstrated moderate yet stable binding, supporting their role as balanced multi-target cosmeceutical candidates. Structure–activity relationship analysis revealed that structural hybridization, π-conjugated systems, electron-donating substituents, and polar functional groups significantly enhance ligand–protein interactions through π–π stacking, hydrogen bonding and electrostatic forces.

Keywords: Anthraquinone hybrids; Anti-aging agents, Anti-acne compounds; Beauty molecules; Cosmetic likeness; Skin care applications.

INTRODUCTION

The development of cosmetic products necessitates rigorous scientific evaluation to ensure consumer safety and compliance with regulatory standards. Prior to market authorization, formulations must undergo comprehensive safety assessment based on the toxicological profiles of individual ingredients, taking into account concentration, exposure conditions, and intended use. Critical endpoints include skin and eye irritation, sensitization, dermal penetration, and carcinogenic potential. In this context, anthraquinones have attracted considerable attention as multifunctional bioactive compounds in cosmetic science due to their antioxidant, photoprotective, and chromophoric properties.[1-2] Structurally defined by a 9,10-anthracenedione core comprising three fused aromatic rings with carbonyl groups at C-9 and C-10, these naturally occurring polyketides are widely distributed in plants such as *Rheum*, *Cassia*, *Aloe*, *Rhamnus*, *Rubia*, and *Morinda*. Representative compounds, including emodin, aloe-emodin, rhein, chrysophanol, and physcion, possess highly conjugated planar structures with hydroxyl or methoxy substitutions that confer redox activity, UV-visible absorption, and the ability to interact with diverse biological targets. These properties underpin their potential in cosmetic applications, particularly in modulating oxidative stress and inflammatory pathways, thereby mitigating collagen degradation and UV-induced skin damage.[3-4] Additionally, certain derivatives influence melanogenesis and function as natural colorants. The present study evaluates the cosmeceutical potential of anthraquinone derivative, organized into Group I [emodin (**1**-**14**) and 4-amino-emodin (**15**-**24**)], Group II [aloe-emodin-coumarin (**25**-**37**) and aloe-emodin-pyrazole hybrids (**38**-**53**)], and Group III [rhein derivatives (**54**-**85**)] (Figure 1).[5-9]

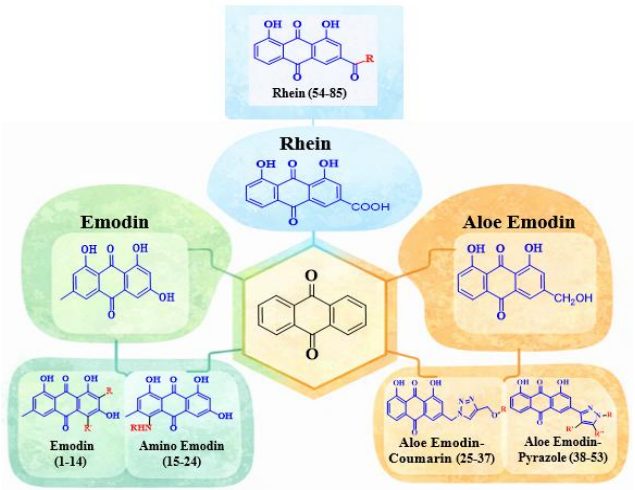

Figure 1: Anthraquinone derivatives.

These compounds were systematically evaluated for their anti-aging, anti-acne, anti-pigmentation and anti-inflammatory activities through a structured, multi-stage screening strategy integrating in silico ADMET prediction, safety assessment and molecular docking against selected therapeutic targets, facilitating the prioritization of anthraquinone scaffolds with optimal pharmacokinetic and safety profiles. By streamlining candidate selection and reducing experimental burden, in silico screening facilitates efficient and sustainable innovation.[10] Molecular docking was performed against selected protein targets, MMP-1,

DHFR, TYR and COX-2 to investigate binding interactions and therapeutic relevance. Matrix metalloproteinase-1, implicated in skin aging, mediates the degradation of type I and III collagen in the dermis, leading to wrinkle formation and reduced elasticity; its inhibition is therefore critical for preventing collagen breakdown and photoaging. Dihydrofolate reductase, targeted for antiacne activity, is a key enzyme in folate metabolism that catalyses the production of tetrahydrofolate for thymidine and purine synthesis, thereby supporting DNA replication and bacterial proliferation. Tyrosinase, associated with pigmentation processes, catalyses the oxidation of L-tyrosine and L-DOPA during melanin biosynthesis; its inhibition effectively reduces melanin production and hyperpigmentation. Cyclooxygenase-2, linked to inflammatory responses, is an inducible enzyme that converts arachidonic acid into prostaglandins, thereby mediating inflammation, erythema, swelling and skin irritation, particularly under UV-induced and oxidative stress conditions.

MATERIALS AND METHODS

All the ligands and reference compounds were constructed and energy-minimized using the MM2 force field in Chem3D. Crystal structures of target proteins: MMP-1 (1U4G), DHFR (3FRE), TYR (4P6R), and COX-2 (5F1A) were retrieved from the Protein Data Bank and prepared through removal of co-crystallized ligands and water molecules, followed by addition of polar hydrogens and assignment of partial charges. Molecular docking was performed using Auto Dock Tools,[11] employing a grid-based approach to evaluate binding orientations and affinities. Binding poses were ranked based on predicted free energies, and key interactions were analysed. Docking outcomes were benchmarked against reference ligands. Protein-ligand complexes were visualized using BIOVIA Discovery Studio Visualizer.[12] Furthermore, ADMET properties were predicted using Swiss ADME[13] and Deep-pkCSM.[14]

RESULTS AND DISCUSSION

Pharmacokinetics and safety profiling of Anthraquinone derivatives:

A comprehensive dataset encompassing compound numbers, IUPAC names, chemical structures and binding energies of all derivatives are compiled in Supplementary Table S1. The ADMET evaluation of emodin, Aloe emodin and rhein derivatives highlights distinct yet complementary profiles governing their suitability for topical applications. The emodin derivatives demonstrated favourable dermal characteristics, with 18 moderately soluble and 6 soluble compounds. Their lipophilicity (iLogP: 1.68-3.25) remained within the optimal range for dermal delivery, while TPSA values (87-132.8 Å²) supported efficient membrane permeability. Correspondingly, Log Kp values (-4.95 to -6.71 cm/s) indicated controlled skin penetration, with an inverse relationship observed between TPSA and permeability. The majority of derivatives adhered to Lipinski's rule and generally satisfied additional drug-likeness filters such as Ghose, Veber, Egan and Muegge's confirming favourable pharmacokinetic attributes. Safety profiling revealed that most derivatives were non-skin sensitizing and non-carcinogenic, with all compounds showing acceptable safety for eye corrosion, biodegradability and hERG inhibition. In the Aloe emodin derivatives, clear differences were observed between coumarin and pyrazole hybrids. The coumarin derivatives displayed uniform moderate solubility and optimal lipophilicity (iLogP: 2.61-3.49), but elevated TPSA values (144-168.54 Å²) resulted in lower skin permeability (Log Kp: -6.65 to -7.20 cm/s), favouring localized epidermal retention. In contrast, the pyrazole hybrids exhibited predominantly poor solubility, although this may support prolonged stratum corneum retention and sustained topical release. These compounds showed higher lipophilicity (iLogP: 3.76-4.50), which enhanced membrane affinity and slightly improved permeability (Log Kp: -5.34 to -6.23 cm/s) despite similarly high TPSA (145-168 Å²), indicating that increased lipophilicity partially compensates for polarity. However, formulation strategies such as lipid-based carriers or nano-systems may be required to address solubility limitations. Both Aloe emodin series showed widespread violations of oral drug-likeness filters due to high polarity and molecular bulk, but this property supports dermal localization. Notably, they exhibited the most consistent safety profile, with all compounds predicted as non-skin sensitizing, non-carcinogenic and safe regarding eye corrosion, biodegradation and hERG inhibition, reinforcing their suitability for topical applications. The rhein derivatives displayed the widest physicochemical diversity, with iLogP values ranging from 0.59 to 5.0 and varied solubility profiles from moderate to very soluble. TPSA values (103-193 Å²) contributed to a broad range of skin permeability (Log Kp: -5.27 to -9.19 cm/s), where compounds with TPSA below 140 Å² showed better diffusion, while highly polar derivatives exhibited restricted permeation. Most hybrids complied with Lipinski's rule and other drug-likeness criteria, indicating moderate pharmacokinetic suitability. Safety assessment suggested minimal toxicity, with most derivatives being non-skin sensitizing and non-carcinogenic, and all compounds safe for eye corrosion, biodegradation, and hERG inhibition. Overall, emodin derivatives show balanced ADMET profiles, aloe-emodin hybrids favour dermal retention with high safety, and rhein derivatives offer optimization flexibility, collectively supporting their potential for topical dermatological and cosmeceutical applications.

Molecular docking analysis:

Emodin and amino-emodin derivatives:

The binding energy ranges for the emodin derivatives and amino-emodin hybrids were observed between -6.38 to -10.25 kcal/mol (MMP-1), -7.67 to -11.32 kcal/mol (DHFR), -7.27 to -10.90 kcal/mol (TYR) and -8.35 to -12.20 kcal/mol (COX-2). Among these, compounds **6**, **7**, **9**, **13**, **17**, **19**, and **20** exhibited enhanced binding relative to the parent emodin scaffold, with favourable ADME and safety profiles. Activity within this series is strongly influenced by the type, position and nature of substituents, where aromatic

expansion and electron-donating groups significantly enhance π-π stacking and hydrophobic interactions. Compounds **6**, **7**, and **9** in particular, demonstrated strong multi-target activity (Figure 2), supported by rich interaction profiles including π-π stacking, π-cation, π-anion, alkyl and van der Waals interactions, which collectively stabilize ligand-protein complexes. Notably, compound **9** exhibited the most versatile interaction pattern, incorporating amide π-stacking and π-lone pair interactions, contributing to its superior binding across multiple targets (Figure 3). **7** further benefits from optimal *p*-substitution, improving steric alignment and enhancing DHFR binding while maintaining COX-2 activity. **6** showed strong affinity due to enhanced hydrophobic and π-π interactions driven by the *p*-methyl phenyl group. In contrast, **13** displayed a more selective interaction profile, relying predominantly on π-π stacking and hydrogen bonding interactions, which favour DHFR activity but limit interaction diversity across other targets (Figure 3). Additionally, π-σ and π-lone pair interactions were observed to further stabilize complexes, particularly in MMP-1 and TYR targets. Electron-withdrawing halogens **3** contributed to improved binding through van der Waals and potential halogen bonding interactions, while heteroatom-containing substituents enhanced hydrogen bonding capacity. Overall, the most potent derivatives **6**, **7**, **9** and **13** achieve an optimal balance of hydrophobicity, electronic effects and diverse non-covalent interactions, supporting their potential as promising multi-target candidates for dermatological and cosmeceutical applications (Figure 2).

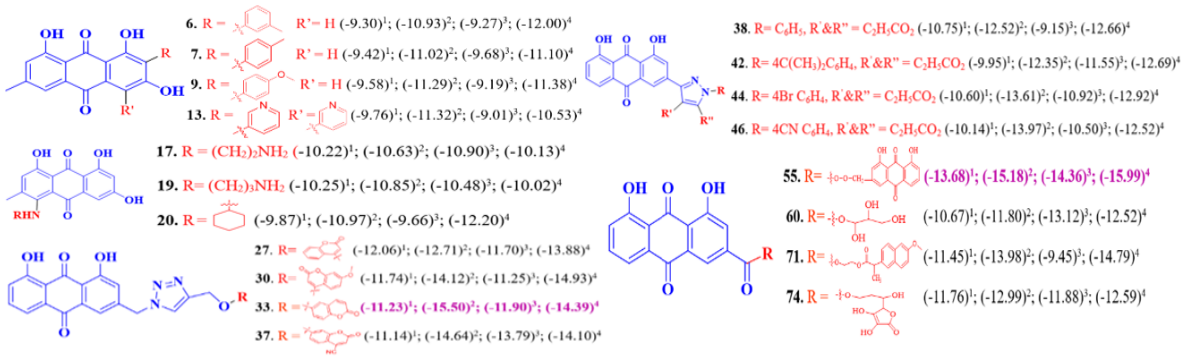

Figure 2: Promising cosmeceutical leads.

The SAR analysis of amino-emodin hybrids indicates that binding affinity is primarily governed by side-chain flexibility, polarity and the nature of substituents. The parent-like amino derivative **15** showed only moderate activity, suggesting that the core scaffold provides essential hydrogen bonding but lacks sufficient hydrophobic complementarity. Introduction of hydroxyl-bearing side chains **16** improved affinity, particularly toward DHFR and COX-2, due to enhanced hydrogen-bond stabilization. A marked improvement was observed with flexible amino-alkyl substitutions, where **17** demonstrated strong and consistent multi-target activity. This is attributed to optimal chain length and terminal amine functionality, enabling effective hydrogen bonding and electrostatic interactions. Its rich interaction profile, including π-cation, π-anion, amide π-stacking and π-alkyl contacts, contributes to stable ligand-protein complexes. Similarly, **19** exhibited excellent broad-spectrum affinity, where increased chain length enhances conformational adaptability and binding orientation, supported by hydrogen bonding and π-alkyl interactions. In contrast, the bulky cyclohexyl-substituted **20** showed the highest COX-2 affinity, driven by strong hydrophobic and van der Waals interactions within non-polar pockets. Its interaction profile includes π-cation and amide π-stacking, favouring DHFR and COX-2 targets, although reduced polarity limits activity against other targets. Heterocyclic substitutions (**21**-**22**) maintained moderate activity through balanced steric and polar interactions, whereas rigid fused systems (**23**-**24**) reduced binding due to steric hindrance and limited flexibility. Overall, amino-emodin hybrids achieve optimal multi-target activity through a balance of hydrogen bonding, electrostatic and π-mediated interactions. Flexible amino chains **17**, **19** promote broad-spectrum binding, while bulky hydrophobic groups **20** enhance target-specific affinity, highlighting the importance of tuning chain length, polarity, and steric features for multifunctional optimization (Figure 2).

Aloe emodin derivatives:

Aloe emodin-coumarin derivatives:

The Aloe emodin-coumarin hybrids exhibited strong docking scores across all targets, ranging from -10.66 to -12.06 kcal/mol (MMP-1), -12.71 to -15.50 kcal/mol (DHFR), -10.34 to -13.79 kcal/mol (TYR), and -13.67 to -14.93 kcal/mol (COX-2), indicating highly stable ligand-protein interactions. Among these, **27**, **30**, **33** and **37** emerged as promising multifunctional leads. SAR analysis revealed that hybridization of the aloe-emodin core with the coumarin pharmacophore *via* a triazole linker significantly enhances binding affinity compared to the parent scaffold. The planar anthraquinone nucleus enables π-π stacking and hydrogen bonding, while the coumarin moiety extends into hydrophobic sub-pockets, increasing van der Waals and aromatic interactions. Even the unsubstituted analogue **25** demonstrated strong multitarget activity, confirming the intrinsic advantage of this hybrid framework. Substituent effects on the coumarin ring critically modulate activity. *p*-substituted derivatives generally exhibited superior binding due to optimal planarity and extended π-conjugation,

whereas *m*-substitution caused slight reductions due to minor steric misalignment and *o*-substitution led to decreased affinity due to steric hindrance. Electron-withdrawing groups (e.g., -Cl, -Br, -NO_2) enhanced binding through increased polarizability and dipole interactions, particularly for DHFR and COX-2 targets, while electron-donating groups (-OCH_3, -CH_3) supported balanced multi-target activity. **27** and **30** demonstrated strong MMP-1 and COX-2 affinities, respectively, driven by improved hydrophobic surface area and electronic effects. Notably, **33** showed the highest DHFR activity, attributed to its fused aromatic system that maximizes π-π stacking and polar anchoring (Figure 4-ii).

Similarly, **37** exhibited the best TYR activity, where the cyano substituent enhances dipolar interactions and target selectivity. Interaction profiling further corroborates these SAR trends. **31** and **33** displayed rich interaction networks involving π-π stacking, π-cation/anion and π-donor interactions, significantly improving binding stability (Figure 3). **30** achieved balanced affinity through π-σ and amide-π stacking interactions, supporting effective ligand anchoring, while **37** benefited from π-π stacking and π-lone pair interactions, enhancing electronic complementarity and binding orientation. Across the series, alkyl and π-alkyl interactions contribute to hydrophobic stabilization, while carbon-hydrogen bonds fine-tune ligand positioning. Collectively, the synergy of aromatic extension, substituent effects, and diverse non-covalent interactions underpins the strong multi-target potential of Aloe emodin-coumarin hybrids for dermatological and cosmeceutical applications (Figure 2).

Aloe emodin-pyrazole derivatives:

The Aloe emodin-pyrazole hybrids exhibited notable binding affinities across all targets, ranging from -8.95 to -10.75 kcal/mol (MMP-1), -11.86 to -13.97 kcal/mol (DHFR), -9.06 to -11.55 kcal/mol (TYR), and -11.04 to -12.92 kcal/mol (COX-2), highlighting **38**, **42**, **44** and **46** as key multifunctional candidates. Overall, hybridization with the pyrazole ring significantly enhances activity by introducing additional π-conjugation, hydrogen bonding sites, and structural rigidity, thereby improving ligand orientation and enabling stable π-π stacking, hydrophobic and polar interactions within the binding pockets. Substituent variation on the terminal phenyl ring plays a critical role in modulating activity. The unsubstituted phenyl derivative **38** demonstrated balanced multi-target binding, supported by a diverse interaction profile including π-π stacking, π-cation and π-anion interactions, ensuring stable ligand-protein complexes (Figure 3).

Electron-donating groups -CH_3 (**41**) and -OCH_3 (**47**) maintained good activity, particularly for DHFR targets, by enhancing electron density and hydrophobic interactions, though with slightly reduced TYR affinity. In contrast, bulky hydrophobic substituents such as *tert*-butyl **42** improved TYR and COX-2 activity through enhanced hydrophobic pocket occupancy, albeit with a simpler interaction profile dominated by hydrogen bonding and π-alkyl contacts. Electron-withdrawing substituents significantly improved binding affinity, particularly for DHFR and COX-2 targets. The bromo-substituted **44** showed strong activity due to enhanced van der Waals interactions and potential halogen bonding. Notably, the cyano-substituted **46** emerged as the most potent DHFR candidate with a rich interaction network involving π-π stacking, π-anion and amide-π interactions, which collectively enhance ligand stabilization and binding specificity.

Variations in ester groups had minimal impact, although bulkier ethyl esters slightly favoured hydrophobic interactions. Across the series, π-σ and π-alkyl interactions consistently contribute to hydrophobic stabilization, while amide π-stacking and hydrogen bonding enhance binding specificity and orientation. Overall, electron-withdrawing substituents (-CN, -Br) drive higher binding affinity, whereas unsubstituted and moderately electron-donating groups support balanced multi-target activity. **38** and **46**, in particular, exhibit optimal interaction diversity and binding strength, underscoring the importance of tuning electronic and steric factors in designing effective multifunctional dermatological agents (Figure 2).

Rhein derivatives:

The rhein hybrids demonstrated a wide range of binding affinities across all targets, with docking scores of -6.20 to -13.68 kcal/mol (MMP-1), -9.23 to -15.18 kcal/mol (DHFR), -2.05 to -14.36 kcal/mol (TYR), and -9.50 to -15.99 kcal/mol (COX-2). Among these, **55**, **60**, **71** and **74** emerged as the most promising multi-target candidates, highlighting the rhein scaffold as a versatile platform for multifunctional dermatological and cosmeceutical development. SAR analysis indicates that substitution at the rhein carboxyl group critically governs activity by modulating aromaticity, polarity and steric effects. Compound **55** exhibited the highest binding across all targets, attributed to its extended polyaromatic system and multiple hydroxyl groups, which promote strong π-π stacking, hydrogen bonding, and electrostatic interactions. Its rich interaction profile, including π-cation/anion and π-donor interactions, enables superior ligand stabilization and consistent multi-target potency (Figure 4- i, iii and iv). Similarly, **71**, bearing a bulky aromatic substituent, showed strong DHFR and COX-2 activity, supported by extensive π-π stacking and π-cation interactions, although slight steric hindrance reduced TYR affinity. In contrast, **60**, with an aliphatic hydroxyl-containing substituent, exhibited moderate binding due to reduced aromaticity, relying mainly on hydrogen bonding, van der Waals, and amide π-stacking interactions. **74** demonstrated balanced activity across all targets, where its polar yet compact structure supports hydrogen bonding and moderate π-σ and π-alkyl interactions, enabling stable but less interaction-rich binding. Hybrids with long flexible chains **61**-**63** or bulky heterocyclic amines **64**-**66**, **69** showed variable or reduced activity due to increased flexibility, steric hindrance or suboptimal binding orientation (Figure 2). Overall, the SAR highlights that optimal activity in rhein hybrids is achieved through a balance of extended

aromaticity, moderate polarity and controlled steric bulk. Interaction diversity particularly π-driven and hydrogen bonding interactions directly correlates with binding strength, establishing compound **55** as the most potent and versatile multi-target lead.

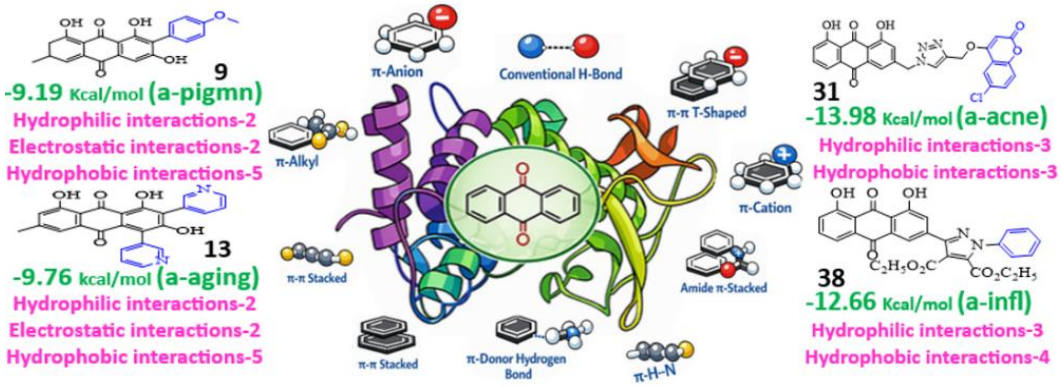

Figure 3: Various stabilizing interactions of representative compounds with target proteins: **9** (TYR), **13** (MMP-1), **31** (DHFR), and **38** (COX-2).

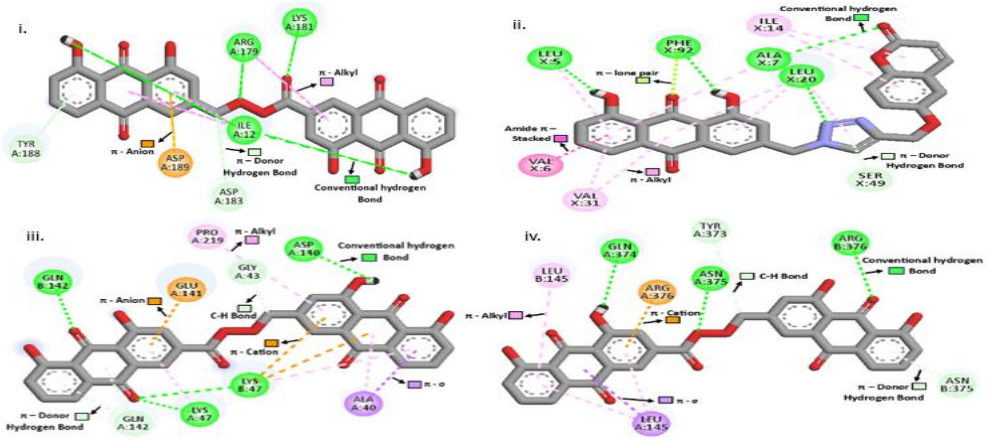

Figure 4: 2D interaction maps of the top-performing compounds: i. **55**-MMP1, ii. **33**-DHFR, iii. **55**-TYR, iv. **55**-COX-2.

Compounds **55** and **33** emerged as the top multi-target leads, exhibiting excellent binding across all four proteins. **55** showed the highest overall affinity, driven by extensive hydrogen bonding, π-cation/π-anion, and electrostatic interactions that promote strong and stable binding within active sites. In comparison, **33** also demonstrated high potency, primarily supported by π-π stacking, π-π T-shaped, and amide-π interactions arising from its coumarin framework, which favours aromatic-rich environments. Overall, **55** is predominantly polar interaction-driven and represents the most potent lead, whereas **33** is π-interaction-driven, making both promising and complementary templates for multifunctional dermatological drug design. include the reference and parent molecules. Emodin, aloe-emodin and rhein derivatives exhibited improved pharmacokinetic profiles and enhanced therapeutic potential compared to both the parent scaffolds and conventional reference hydroquinone.

CONCLUSION

In this study, we have validated a series of emodin, aloe-emodin and rhein derivatives for their cosmeceutical applications such as anti-aging, anti-acne, anti-pigmentation and anti-inflammatory through systematic molecular docking and ADMET analysis, evaluating their multi-target dermatological potential. The results demonstrated that structural hybridization significantly enhances binding affinity and functional versatility. Among the series, aloe-emodin-coumarin and rhein derivatives exhibited superior cosmeceutical activity, with compounds **33** and **55** identified as the most promising multi-target leads. SAR analysis indicated that π-conjugated systems, electron-donating substituents and polar functional groups play a crucial role in optimizing ligand-protein interactions. ADMET studies further supported their suitability for topical applications, highlighting favourable lipophilicity, controlled skin permeability and robust safety profiles. While aloe-emodin hybrids favour localized dermal retention, rhein derivatives offer structural diversity for fine-tuning pharmacokinetic properties. Overall, these findings establish anthraquinone hybrids as versatile and promising candidates for the development of multifunctional dermatological and cosmeceutical agents, warranting further experimental validation and formulation optimization for practical applications.

Source of Support: The author(s) received no financial support for the research, authorship, and/or publication of this article

Conflict of Interest: The author(s) declared no potential conflicts of interest with respect to the research, authorship, and/or publication of this article.

REFERENCES

1. Malik EM, Müller CE, Anthraquinones As Pharmacological Tools and Drugs, Med Res Rev, 2016; 36(4):705-48. https://doi.org/10.1002/med.21391.
2. Chwan-Fwu L, Shih-Yi C, Tse-Hung H, Thi MHN, Pei-Wen W, Ahmed A, Jia-You F, A systematic comparison of the effect of topically applied anthraquinone aglycones to relieve psoriasiform lesion: The evaluation of percutaneous absorption and anti-inflammatory potency, Biomed. Pharmacother, 2022; 145:112482. https://doi.org/10.1016/j.biopha.2021.112482.
3. Hua-jin Z, Dong-qin S, San-hui C, Jun-jun Z, Gui-zhou H, Ran Y, Inhibitory effects of four anthraquinones on tyrosinase activity: Insight from spectroscopic analysis and molecular docking, Int. J. Biol. Macromol, 2020; 160:153-163. https://doi.org/10.1016/j.ijbiomac.2020.05.193.
4. Khan N, Karodi R, Siddiqui A, Thube S, Rub R, Development of anti-acne gel formulation of anthraquinones rich fraction from Rubia cordifolia (Rubiaceae), Int. J. Appl. Res. Nat. Prod, 2012; 4(4):28-36,
5. Steffi KK, Jun-ichi H, Sha B, Finith EJ, Miwa O, Chieko K, Emi S, Vikas PS, Lijun S, Design and synthesis of emodin derivatives as novel inhibitors of ATP-citrate lyase, Eur. J. Med. Chem, 2017; 126:920-928. https://doi.org/10.1016/j.ejmech.2016.12.018.
6. Teich L, Daub KS, Krügel V, Nissler L, Gebhardt R, Eger K, Synthesis and biological evaluation of new derivatives of emodin, Bioorg Med Chem, 2004; 12(22):5961-71. https://doi.org/10.1016/j.bmc.2004.08.024.
7. Shang H, Hu Y, Li J, Li L, Tian Y, Li X, Wu Q, Zou Z, The Synthesis and Biological Evaluation of Aloe-Emodin-Coumarin Hybrids as Potential Antitumor Agents, Mol, 2022; 27:6153. https://doi.org/10.3390/molecules27196153.
8. Guddeti DK, Bandi S, Sravanthi V, Surendar RB, Hashnu D, Suresh BK, Design, synthesis, and biological evaluation of pyrazole-linked aloe emodin derivatives as potential anticancer agents, RSC Med Chem, 2021; 12:791-796. https://doi.org/10.1039/D0MD00315H.
9. Zhang Y, Jiang Y, Shang K, Ge C, Fang J, Liu S, Updated pharmaceutical progress on plant antibiotic rhein and its analogs: Bioactivities, structure-activity relationships and future perspectives, Bioorg Med Chem, 2024; 113:117895.
10. Immaculate A, Kalpana A, In Silico Analysis of Flavonoid–Triazole Hybrid Inhibitors Targeting Neurodegenerative, Oncological, and Infectious Diseases, Int. J. Pharm. Sci. Rev. Res, 2026; 17:139-147. DOI: 10.47583/ijpsrr.2026.v86i04.017
11. Morris GM, Goodsell DS, Halliday RS, Huey R, Hart WE, Belew RK, Automated docking using a lamarckian genetic algorithm and an empirical binding free energy function, J. Comput. Chem, 1988; 19:1639-1662.
12. Dassault Systèmes: BIOVIA Discovery Studio Visualizer 2021. Available online: https://discover.3ds.com/discovery-studio visualizer-download (accessed on 15 March 2023).
13. Daina A, Michielin O, Zoete V, SwissADME: a free web tool to evaluate pharmacokinetics drug-likeness and medicinal chemistry friendliness of small molecules, Sci. Rep, 2017; 7:42717. https://doi.org/10.1038/srep42717.
14. Myung Y, De Sá AGC, Ascher DB, Deep-PK: Deep Learning for Small Molecule Pharmacokinetic and Toxicity Prediction, Nucleic Acids Res, 2024; 52:W469-W475. https://doi.org/10.1093/nar/gkae254.